Clinical Neurophysiology 125 (2014) 83–97

Contents lists available at SciVerse ScienceDirect

Clinical Neurophysiology

journal homepage: www.elsevier.com/locate/clinph

Group Independent Component Analysis (gICA) and Current Source Density (CSD) in the study of EEG in ADHD adults

Valery A. Ponomarev [a,*], Andreas Mueller [b], Gian Candrian [b], Vera A. Grin-Yatsenko [a], Juri D. Kropotov [a]

[a] N.P. Bechtereva Institute of the Human Brain of Russian Academy of Sciences, St. Petersburg, Russia
[b] Brain and Trauma Foundation Grisons, Chur, Switzerland

ARTICLE INFO

Article history:
Accepted 21 June 2013
Available online 16 July 2013

Keywords:
Group Independent Component Analysis
Current Source Density
ADHD
EEG spectra

HIGHLIGHTS

- ADHD adults showed reduced EEG activity in the different frequency ranges as compared with healthy subjects.
- Spatial pattern of differences depended on whether the eyes were open or closed.
- gICA and CSD approaches are probably more sensitive for differentiating the characteristics of EEG spectra in groups of patients/subjects, as compared to spectral analysis of EEG.

ABSTRACT

Objective: To investigate the performance of the spectral analysis of resting EEG, Current Source Density (CSD) and group independent components (gIC) in diagnosing ADHD adults.
Methods: Power spectra of resting EEG, CSD and gIC (19 channels, linked ears reference, eyes open/closed) from 96 ADHD and 376 healthy adults were compared between eyes open and eyes closed conditions, and between groups of subjects.
Results: Pattern of differences in gIC and CSD spectral power between conditions was approximately similar, whereas it was more widely spatially distributed for EEG. Size effect (Cohen's *d*) of differences in gIC and CSD spectral power between groups of subjects was considerably greater than in the case of EEG. Significant reduction of gIC and CSD spectral power depending on conditions was found in ADHD patients. Reducing power in a wide frequency range in the fronto-central areas is a common phenomenon regardless of whether the eyes were open or closed.
Conclusions: Spectral power of local EEG activity isolated by gICA or CSD in the fronto-central areas may be a suitable marker for discrimination of ADHD and healthy adults.
Significance: Spectral analysis of gIC and CSD provides better sensitivity to discriminate ADHD and healthy adults.

1. Introduction

Attention-Deficit Hyperactivity Disorder (ADHD) is a childhood psychiatric disorder which is characterized by excessive restlessness, poor concentration, impulsive and hyperactive behavior (DSM-IV, American Psychiatric Association, 1994) and affects 5–10% of the population (Spencer et al., 2007). From 35% to 80% of children with ADHD continue to manifest symptoms in adulthood (Gittelman et al., 1985; Barkley et al., 1990, 2008; Faraone et al., 2006; Spencer et al., 2007; Biederman et al., 2010). Along with the patients meeting the diagnostic criteria of ADHD there is quite a large amount of individuals displaying some of the symptoms of ADHD, but failing to meet the diagnostic criteria of this disorder. The patients belonging to this subclinical group of ADHD still suffer significant maladjustment and like individuals with ADHD face problems with peer and family relations, difficulties in academic performance and employment functioning (Barkley et al., 2006).

In the last decades, quantitative measurements based on the spectral analysis of EEG recordings are widely used to determine the neural correlates of ADHD. These studies of children and adolescents with ADHD have reported increased power in the slow EEG frequency bands (predominantly theta band) and reduced power of beta activity as compare to normal controls (Chabot and Serfontein, 1996; Clarke et al., 2002; Barry et al., 2003).

* Corresponding author. Address: Laboratory of Neurobiology of Action Programming, N.P. Bechtereva Institute of the Human Brain of Russian Academy of Sciences, 197376, St. Petersburg, ul. Acad. Pavlova, 9, Russia. Tel.: +7 921 438 02 19; fax: +7 812 234 32 47.
E-mail address: valery_ponomarev@mail.ru (V.A. Ponomarev).

1388-2457/$36.00
http://dx.doi.org/10.1016/j.clinph.2013.06.015

Table 1
EEG findings in EEG spectra studies in ADHD adults.

References	(a) Referent; (b) EOG exclusion criteria. (c) Spectra computation	Subject groups: number of subjects per group	Condition, task	Sites	δ	θ	α	β
Bresnahan et al. (1999)	(a) Linked ears. (b) ±100 μV (c) 2 s; NE ⩾ 15	ADHD, control: Children: 25, 25, Adolescent: 25, 25, adults: 25, 25.	EO, fixate on monitor	Fz, Cz, Pz	↑*** In all sites Pz dominant	↑*** In all sites Pz dominant	–	–
Bresnahan and Barry (2002)	(a) Linked ears. (b) ±100 μV (c) 2 s; NE ⩾ 15	ADHD, non-ADHD, control: 50, 50, 50	EO. fixate on monitor	Fz, Cz, Pz	↑* In all sites Fz dominant	↑*** In all sites	↑* In all sites Pz dominant	↑*** Pz
Bresnahan et al. (2006)	(a) Linked ears. (b) ±100 μV (c) 2 s; NE ⩾ 15	ADHD, control: 50, 50	EO, fixate on monitor	Fz, Cz, Pz	↑* In all sites	↑*** In all sites	–	–
Hermens et al. (2004)	(a) Linked ears. (b) EOG correction (c) 2 s; NE = 60	ADHD, control Male: 21, 21, Female: 14, 14	EC, simply sit	Fz, Cz, Pz	↑*	↑* (male only) In all sites,	–	↓* Pz
				Anterior/ posterior	↑*	↑* (male only) In all sites		↓** Posterior
Koehler et al. (2009)	(a) Average (b) ±100 μV (c) 2 s; NE ⩾ 40;	ADHD, control: 34, 34	EC, do not move eyes.	Anterior/ central/ Posterior	–	↑* Posterior	↑** Posterior	–
Loo et al. (2009)	(a) Linked ears. (b) Visual exclusion. (c) 1 s; unknown	ADHD, control: 38, 42	EO, unknown EC, unknown	Frontal/ parietal	–	–	↓** Frontal	↑* In all sites
Liechti et al. (2013)	(a) Linked ears or average (b) ±50 μV or ICA based correction. (c) 2 s; NE ⩾ 20	ADHD, control: 32, 30	EO, fixate on monitor EC, do not move eyes.	Fz, Cz, Pz	– –	– –	– –	– –

↑*, ↑** and ↑*** – increased in ADHD with $p < 0.05$, $p < 0.01$ and $p < 0.001$ correspondingly; ↓*, ↓** and ↓*** – decreased in ADHD. δ, θ, α and β – delta, theta, alpha and beta frequency ranges correspondingly. "(c) Spectra computation" includes (1) – the duration of epoch for Fourier transformation; (2) – the minimum number of average epochs for each individual spectrum (NE).

Increased theta activity is associated with under-arousal and indicative of decreased cortical activity (Chabot and Serfontein, 1996; Clarke et al., 1998; Lazzaro et al., 1998; El-Sayed et al., 2002).

Until now, only a few studies have been carried out in adult ADHD patients, and their results are largely inconsistent (see Table 1). For example, some researchers have reported the increase in the theta band power at rest in ADHD adults (Bresnahan et al., 1999, 2006; Bresnahan and Barry, 2002; Hermens et al., 2004; Koehler et al., 2009). However, other authors found no statistically significant change in the theta level (Loo et al., 2009; Liechti et al., 2013). The picture is similar for the delta, alpha and beta band power (see Table 1). The diversity and inconsistency of these EEG findings underscores importance of further research to clarify the changes of EEG in adult ADHD patients.

Such a variety of observations can be explained by methodological differences in the analysis of EEG, or by subtle dissimilarity of the criteria used to select the groups of patients and healthy subjects, or by accidental causes when multiple comparisons (i.e. total number of comparisons in several series of experiments) were performed. For the latter reason, a similar phenomenon can be observed when there are no real differences, and when they have a small effect size. Indeed, most studies have shown significant differences at $p < 0.05$ or $p < 0.01$, which approximately corresponds to a "small" effect size for a given number of subjects (see Table 1). Thus, without diminishing the value and importance of these studies, one can conclude that the spectral analysis of the EEG at rest has low sensitivity to discriminate ADHD and control groups (Liechti et al., 2013).

The differences in the EEG spectral power may have a "small" effect size, if they are really small, or if they are hidden by large between-subject variability, or if large local changes of the EEG activity are masked by signals propagating through the volume conduction from neighboring brain areas. If the latter assumption is correct, then higher sensitivity can be achieved using the methods, which minimize the volume conduction effects. One possible approach is based on transformation of EEG scalp potentials into Current Source Density (CSD) and the subsequent analysis of its spectral power (see Tenke and Kayser, 2005, for a detailed discussion). Several algorithms based on the linear volume-conduction model have been previously proposed to transform the data into the CSD (Hjorth, 1975, 1980; Perrin et al., 1989; Yao, 2002). They compute an estimate of the radial component of current (i.e. the surface Laplacian) that penetrates through the skull and scalp from underlying neural tissue at a given point on the scalp.

Another possible approach, including the Independent Component Analysis (ICA), is a modeling the original EEG as a linear combination of mutual statistically independent or weakly correlated components. This approach is not based on the physical principles, and the resulting model does not describe directly the properties of the electrical conductivity of the head, but it can be very effective for minimizing interference of the fields of neighboring brain areas, when volume conduction provides a considerable contribution to the mutual dependence of EEG signals. As it was shown in numerous studies, ICA have provided a functionally relevant analysis of brain activity (Makeig et al., 1996, 1997; Hyvärinen and Oja, 2000; Vigário et al., 2000; Debener et al., 2005; Onton and Makeig, 2006; Onton et al., 2006; Congedo et al., 2010a,b; Makeig and Onton, 2012). The successful application of ICA in some clinical studies such as Alzheimer's disease (Melissant et al., 2005), epilepsy (Leal et al., 2006; Iriarte et al., 2006; Marques et al., 2009), Creutzfeldt–Jakob disease (Hung et al., 2007), autism (Milne et al., 2009), obsessive–compulsive disorder (Kopřivová et al., 2010), traumatic brain injury (Cao and Slobounov, 2010), and depressive disorder (Grin-Yatsenko et al., 2010) has been reported.

The simplest mixture model $x(t) = As(t)$ is assumed in the case of ICA, where the output $x(t)$ is $n \times 1$ vector of measured data points at time instant t ($t = 1,\ldots,T$), A is $n \times n$ mixing matrix and $s(t)$ is $n \times 1$ vector of independent components. If A is invertible than the sources $s(t)$ can be estimates as $s(t) = Wx(t)$, where $W = A^{-1}$ is unmixing matrix. Several methods have been proposed to find matrix W or A (see Comon and Jutten, 2010 for a detailed discussion) including InfoMax algorithm (Bell and Sejnowski, 1995).

ICA is usually applied to single subject data (iICA) because it is assumed a priori that the set of brain sources and their spatial location can vary from person to person (Makeig and Onton, 2012). This approach allows revealing dependence of the signals on the experimental conditions for each subject separately, and the further generalization for the entire group of subjects can be performed using clustering technique. However, it is well known that output independence leads to a matrix W that satisfies $WA = PD$, where P is a permutation matrix and D is a diagonal matrix, i.e. estimated outputs are equal to the sources, up to a permutation and a scale (Comon, 1994). This ambiguity leads to the serious problems when comparing the signals obtained by two or more ICA decompositions.

Several methods have been proposed to overcome this ambiguity, which are usually called as Group Independent Component Analysis (gICA). However, such methods are based on additional assumptions. For example, an elegant gICA method (Eichele et al., 2011) supposes that the signals have to be time- and phase-locked within and across subjects. This method may be very effective in the analysis of event-related EEG data, but it is not suitable for the analysis of the background rhythmic activity. Other gICA methods (Congedo et al., 2010a,b; Grin-Yatsenko et al., 2010) assume that the mixing process (i.e. matrix A) is the same for all subjects. The main difference between these methods is the technique for assessing the mixing matrix. The former authors used the de-correlation technique based on second order statistics in the frequency domain (Congedo et al., 2008). This approach has a serious drawback: it cannot separate sources if at least two of them have identical temporal correlation structure, i.e. proportional power spectra (Yeredor, 2010). Inasmuch as the shape of the EEG power spectra is approximately the same for the electrodes placed symmetrically to the median line of the brain, this limitation of such methods seems to be critical (Hyvärinen et al., 2010). Other authors (Grin-Yatsenko et al., 2010) used the InfoMax algorithm (Bell and Sejnowski, 1995) in the time domain, which is free from the above drawbacks. Unfortunately, the latter method also has its limitations (see below).

Strictly speaking, the assumption regarding the identity of mixing processes in all subjects may be a rather rough approximation (see Makeig and Onton, 2012, for a detailed discussion). But it is also possible that the number of sources is the same for all subjects, their spatial localization differ relatively little from each other, and their small displacements in relation to the sensors may have a minor effect on the EEG signals at least in the case of a low-density electrode grid. For these reasons, we suppose that mixing processes is approximately the same for all subjects, but this assumption must be verified.

The assumptions underlying ICA is as follows: (1) the sources are statistically independent, (2) the mixing process is linear and instantaneous, (3) each source signal can be modeled as an independent and identically distributed (i.i.d.) process, (4) the sources have non-Gaussian probability density functions and (5) the number of independent sources is the same as the number of sensors. The correspondence between these assumptions and the dynamics of brain electrical processes is analyzed in several studies (James and Hesse, 2005; Onton and Makeig, 2006; Congedo et al., 2008; Makeig and Onton, 2012). Briefly it can be summarized as follow: the assumption (1) seems to be satisfied as an approximation in the meaning that the complexity of EEG dynamics can be modeled, at least in part, as a collection of a modest number of statistically independent brain processes. The assumption (2) can be also satisfied since volume conduction in brain tissue, at the EEG frequencies, is effectively instantaneous and almost linear. But, taking into account the neuronal interconnections this assumption should be considered as an approximation. The assumption (3) is clearly not satisfied, since the brain signals have considerable autocorrelation and cannot be modeled as i.i.d. processes. In particular it has been shown that, if strong time dependencies are present in the data, the ICA source estimates are not reliable (Sarela and Vigario, 2003), because the effective number of i.i.d. samples is too small. The assumption (4) is probably satisfied because the EEG processes have oscillatory nature. The assumption (5) is questionable, since it is well known that the EEG is temporal and spatial non-stationary, and it is very likely that quite a large number of statistically independent sources may be necessary to accurately describe this complex process.

Thus, there are at least two problems when comparing the results of iICA and gICA that cannot be ignored. First, the estimates of mixing matrices will have a large statistical error in the case of iICA, because the EEG recording for each subject is usually too short. Second, it is very probable that the actual number of existing sources is greater than the number of sensors. Then the components resulting from ICA will be a linear combination of signals from the sources with weights varying from subject to subject in an unpredictable way. For these reasons, the differences of mixing matrices can be interpreted either as actually existing, or as a result of the influence of random factors. Apparently, the assessment of how well the mixing matrix obtained for the training data set will fit any other test data sets, will give less ambiguous results.

In summary, the literature review has shown that the spectral analysis of the resting EEG seems to have a low sensitivity for reliable discrimination adult ADHD patients. It is possible that the spectral analysis of the CSD or gICA approach can provide greater sensitivity. However, the gICA approach requires additional validation. Therefore, it is necessary, first, to compare the results the iICA and gICA, and second, to evaluate the advantages and disadvantages of the gICA approach in the context of a well-known phenomena in the case when comparing the spectral power between the eyes open (EO) and eyes closed (EC) conditions.

2. Methods

2.1. Patients and control subjects

96 adults (mean age 36.4; range 20–50, SD 8.36) with symptoms of AD(H)D participated in our study. Subjects were 50 males (mean age 35.7; range 20–48) and 46 females (mean age 37.1; range 22–50). Inclusion in the ADHD group was based on the DSM-IV criteria for ADHD (American Psychiatric Association, 1994). Due to the adult sample, the DSM-IV criteria were modified on one point according to Barkley et al. (2008): the DSM-IV primarily requires that an individual have at least 6 of 9 listed symptoms of inattention or 6 of 9 listed hyperactive/impulsive symptoms to qualify for the diagnosis of ADHD. In the present study, subjects were included in the ADHD group if they retrospectively recalled the presence of at least 4 frequently occurring inattention and/or hyperactivity/impulsivity symptoms in childhood (ages 5–12 years), and if at least 4 inattention and/or hyperactivity/impulsivity symptoms had been frequently present during the past 6 months before study participation. The clinical assessment included a series of ADHD questionnaires, as well as a diagnostic interview. The determination of the presence of ADHD symptoms

in the clinical interview resulted in 23 subjects being the inattentive, 7 subjects being the hyperactive/impulsive, and 66 subjects being the combined ADHD subtype. Again, the presence of 4 symptoms on the inattention and/or the hyperactive/impulsive lists were used as basis for the subtype classification. Subjects were included in the ADHD group only if they had been diagnosed with ADHD prior to study participation by an independent psychiatrist. 63 subjects had been diagnosed with ADHD according DSM-IV criteria. 33 patients belonged to the subclinical group and met less strict criteria described above. Most patients were unmedicated. Those of them who received methylphenidate had withhold from taking this medicine during 24 h before testing. Subjects taking other psychotropics were not included in the study. Also, subjects which had suffered of a head injury with subsequent loss of consciousness, and subjects suffering from neurological or systemic medical diseases were excluded from the study.

The control group included 376 healthy subjects (mean age 32.1; range 20–50, SD 10.2): 167 males (mean age 32.0; range 20–50) and 209 females (mean age 32.1; range 20–50). These were subjects who participated in a project of collecting a reference database. The project was sponsored by the Brain and Trauma foundation from Switzerland. Healthy subjects were recruited from several sources: (1) students of Department of Biology of St. Petersburg State University, (2) scientific staff of the Institute of the Human Brain of Russian Academy of Sciences (in both cases recordings were made by Drs. E.A. Yakovenko and I.S. Nikishena from the Institute of the human Brain), (3) students of Department of Psychology of the Norwegian University of Science and Technology, Trondheim (recording were made by S. Hollup and his students from the Department of Psychology), (4) subjects from Chur, a town near Zurich, recruited by Andreas Mueller (recording were made by E.P. Tereshchenko and G. Candrian). The inclusion/exclusion criteria were: (1) an uneventful perinatal period; (2) no head injury with cerebral symptoms; (3) no history of neurological or psychiatric diseases; (4) no convulsions; (5) normal mental and physical development; (6) average or better grades in school; (7) no current medication or drugs.

The investigation was carried out in accordance with the declaration of Helsinki. All subjects gave informed consent after the procedures had been fully explained to them.

2.2. EEG recording

EEG was recorded using Mitsar-EEG 201-21 system (Mitsar, Ltd). WinEEG software was used for acquisition and analysis of the data. 19 silver-chloride electrodes were applied according to the International 10–20 system. The input signals referenced to the linked ears were filtered between 0.5 and 50 Hz and digitized at a rate of 250 Hz. The ground electrode was placed on the forehead. All electrode impedances were kept below 5 kΩ. EEG was recorded in Eyes closed (EC) and Eyes open (EO) resting conditions, at least 3 min for every period. Subjects had to sit still and try not to blink or move their eyes. Artifact-contaminated epochs were automatically excluded from further analysis. The artifacts rejection thresholds were set as follow: (1) 50 μV for Fp1 and Fp2 electrodes and 100 μV for other electrodes – for non-filtered EEG, (2) 50 μV – for slow waves extracting by digital filtering in 0–1 Hz band, (3) 35 μV – for fast waves filtered in the band 20–35 Hz. These threshold values were chosen empirically using multiple data processing and subsequent visual inspection. The first test effectively eliminates artifacts related to eye blinks and other rapid movements, but skipping almost all the EEG signals. The second test identifies the artifacts associated with the slow head or body movements. The third test detects high-amplitude myographic artifacts related to the tension of muscles when clenching the teeth, swallowing, etc. Before further processing the entire array of EEG recordings were filtered at 1.5–40 Hz frequency band to minimize overlearning problem in independent component analysis (ICA) algorithm (Sarela and Vigario, 2003). The CSD was calculated by the spherical spline surface Laplacian method of Perrin et al. (1989, 1990) using C++ implementation of functions *GetGH.m* and *CSD.m* from Matlab-based CSD Toolbox (Kayser, 2009) with parameters: 10 cm head radius; 50 iterations; $\lambda = 10^{-5}$; $m = 4$ (Kayser and Tenke, 2006a,b).

2.3. Independent component analysis (ICA)

The estimation of the optimal order of ICA model of EEG (the number of components) was performed using three information-theoretic criteria (ITC): Akaike's information criterion – AIC (Akaike, 1974), Kullback–Leibler information criterion – KIC (Cavanaugh, 1999) and minimum description length criterion – MDL (Rissanen, 1978) which were calculated by the formulas for the real data (Li et al., 2007). Because these formulas are derived on the basis of the i.i.d. sample assumption (Wax and Kailath, 1985), the estimation was performed multiple times using data decimation with different subsampling depth.

Since the ITC are approximate, the effects associated with reducing the dimension of the input data have also been studied. Dimension reduction was performed using principal component analysis (PCA), which is an integral part of many ICA algorithms, and is used for pre-whitening, compressing and denoising the data (see Hyvärinen and Oja, 2000; Comon and Jutten).

The InfoMax algorithm was used, in order to obtain estimates of the unmixing matrix W. We used a C++ implementation of the InfoMax algorithm, which is the part of WinEEG software and it is practically identical to the procedure *runica* from the package EEGLAB (Delorme and Makeig, 2004), except the stopping weight change which was reduced from 10^{-6} (default value) to 10^{-7}, and the maximum number of iterations which was increased from 512 to 3000. As a result of these changes, the algorithm became to work stably in the processing of EEG of different durations varying over a wide range from 60 s to several hours.

The estimation of W matrix was carried out for the EO and EC condition separately. Artifact-contaminated epochs were always excluded from the analysis.

In the case of gICA, all individual EEG recordings were concatenated into one combined time series, which was used for assessment of unmixing matrix W. Thus, W^{EO} and W^{EC} matrices were obtained for EO and EC conditions separately. For iICA, we have retained only those individual EEG recordings in which the total duration of the artifact-free data was longer than 120 s: 104 – for the EO condition, and 177 – for the EC condition. In this case, W_k^{EO} and W_k^{EC} matrices were computed for each individual EEG recording and each condition separately.

Only in the study of the effects associated with the dimension reduction, the mixing matrix A was calculated as Moore–Penrose pseudoinverse of W. However, ITC have shown that the optimum number of components equal to the number of electrodes. Therefore, in this particular case, all matrices W (W^{EO}, W^{EC}, W_k^{EO} and W_k^{EC}) were a square, and the corresponding matrices A (A^{EO}, A^{EC}, A_k^{EO} and A_k^{EC}) were calculated as inverse of W ($A = W^{-1}$). The signals for each individual EEG recordings were computed as $s(t) = Wx(t)$. Because all W are square and invertible matrix, such a transformation is reversible, and it will not result in data loss. In the case of gICA, W^{EO} or W^{EC} were used to transform all EEG recordings into the group independent components (gIC^{EO} and gIC^{EC} models correspondingly). In the case of iICA, each individual EEG recording was transformed into independent component using corresponding W_k^{EO} or W_k^{EC}.

Reliability analysis of ICA decomposition was carried out to assess the accuracy of estimation of A and $s(t)$. Because W is the inverse of A, estimation accuracy of $s(t)$ depends on how precisely all

elements of A were evaluated. Therefore, the reliability was assessed for the entire matrix A. Let us introduce a similarity index of two matrixes A^1 and A^2. The similarity of two topographies of components can be evaluated as $r_{ij}^{12} = |A_i^1 A_j^2|/|A_i^1||A_j^2|$, where i and j – the columns of matrices A^1 and A^2 correspondingly. r_{ij}^{12} is invariant with respect to arbitrary rescaling, attains its maximum (one) only for equivalent topographies and its minimum (zero) for orthogonal topographies. The columns of mixing matrices can be reordered step by step in such a way that the maximal indices r_{ij}^{12} will be placed in the diagonal of matrix $R = \{r_{ij}^{12}\}$. Then, the similarity index of two matrixes A^1 and A^2 can be computed as $\hat{r} = \sum r_{ii}^{12}/n$. $\hat{r}$ reaches its maximum (one) for equivalent A^1 and A^2, and it will be approximately equal to 0.42 if the elements of mixing matrices are random values with Gaussian distribution.

If in practice $\hat{r}$ does not reach its maximum, it is important to know the accuracy of estimates of $s(t)$. It seems intuitively clear that if some components are not precisely assessed, and if the total power of these components is large, then the accuracy of the estimation of other components is also low, because the total power of the signal will be erroneously redistributed among all components. Consequently, the relative proportion of the total variance of components, for which the corresponding topographies were assessed reliably, can be used as a rough indicator of the accuracy of estimates. Denote the percent of the total power of components, for which the r_{ii}^{12} is greater or equal r, as:

$$P_r = \frac{\sum_i (Var_i^1 + Var_i^2) H(r_{ii}^{12} - r)}{\sum_i (Var_i^1 + Var_i^2)} \times 100\%,$$

where $H(x)$ – the Heaviside step function:

$$H(x) = \begin{cases} 0, & x < 0 \\ 1, & x \geqslant 0 \end{cases}$$

and Var_i – the variance of i-th component:

$$Var_i = \frac{1}{nT} \sum_{j=1}^{n} \sum_{k=1}^{T} (A_{ij} s_{ik})^2$$

r is in the range of 0–1 and must be chosen closer to 1 if A and $s(t)$ should be estimated more accurately. In our studies, the value of r was equal to 0.95.

First reliability test was performed for the case of iICA.

Reliability test 1. This test is based on split-half comparisons (Groppe et al., 2009). Each individual EEG recording was divided into two equal halves, the matrices A^1 and A^2 were estimated for each of them separately, and indices $\hat{r}$ and $P_{0.95}$ were computed. The average values of indices $\overline{\hat{r}}$ and $\overline{P_{0.95}}$, and their standard deviations σ_r and σ_P were calculated across the EEG recordings.

Other reliability tests were performed for the case of gICA.

Reliability test 2. This test is largely similar to the previous one. The two non-overlapping segments of EEG with predefined duration TI were randomly selected from each individual EEG recording and placed in two separate groups. The set of segments of EEG within each groups were concatenated into two combined time series, which were used to estimate the matrices A^1 and A^2.

Reliability test 3. This test is based on bootstrap resampling (Müller et al., 2004). The individual EEG recordings were concatenated into one combined time series. Random selection of samples from this combined time series was performed twice with probability p. These two subsets of samples were used to estimate the matrices A^1 and A^2.

Reliability test 4. This test is based on random split-half of the group of subjects (Congedo et al., 2010b). The random split-half division of the subjects group was performed, and then the individual EEG recordings within each subgroup were concatenated into two combined time series, which were used to estimate the matrices A^1 and A^2.

These last three tests were repeated 100 times with corresponding fixed parameters TI, p and the group of subjects, and the average values of indices $\overline{\hat{r}}$ and $\overline{P_{0.95}}$, and their standard deviations σ_r and σ_P were calculated.

Reliability test 5. The following modification of Reliability Test 4 was used to assess the reliability of each component separately. In this case, the matrix A^1 was computed for the entire group of subjects, and the matrix A^2 was estimated for randomly selected half of subjects. Next, reordering of columns of mixing matrix A^2 was performed in accordance with the matrix A^1 (see above), and the indices of similarity r_{ii}^{12} were calculated for each of the topographies separately. This procedure was repeated 100 times, and the average indices $\overline{r_{ii}^{12}}$ and its standard deviations σ_{ii} were computed.

Obviously, gICA approach is an approximation and it is necessary to assess how well the gICA model corresponds to each individual EEG recording, as well as to other data sets. Since the purpose of the ICA is a modeling the data using statistically independent processes, the degree of mutual dependence of signals is a natural measure of how well the model fits the data. To quantify it, second and fourth order measures of statistical dependency can be computed (Anemüller et al., 2003). Second order correlations are taken into account by computing the mean of the absolute values of correlation-coefficients for all component pairs i ≠ j:

$$\rho = \frac{1}{n(n-1)} \sum_{i \neq j} |\rho_{ij}|, \quad \rho_{ij} = \frac{\langle s_i(t) s_j(t) \rangle_T - \mu_i \mu_j}{\sigma_i \sigma_j}, \quad \mu_i = \langle s_i(t) \rangle_T,$$

$$\sigma_i = \sqrt{\langle (s_i(t) - \mu_i)^2 \rangle_T}.$$

Higher order statistical dependencies were evaluated by computing the analog quantity ρ':

$$\rho' = \frac{1}{n(n-1)} \sum_{i \neq j} |\rho'_{ij}|, \quad \rho'_{ij} = \frac{\langle s_i^2(t) s_j^2(t) \rangle_T - \mu'_i \mu'_j}{\sigma'_i \sigma'_j}, \quad \mu'_i = \langle s_i^2(t) \rangle_T,$$

$$\sigma'_i = \sqrt{\langle (s_i^2(t) - \mu'_i)^2 \rangle_T}.$$

Its value is zero for independent signals, non-zero for signals exhibiting correlated fluctuations in signal power, and maximum (one) only for signals with proportional squared-amplitude time-courses.

In the case of gICA, the ρ and ρ' quantities were computed for the raw EEG, the CSD, the gICEO and the gICEC, for healthy subjects and ADHD patients, and for the EO and EC conditions separately. The ρ and ρ' were computed either for the combined time series, or for each individual EEG recording and averaged.

In the case of iICA, the ρ and ρ' quantities were computed for three combinations of training and test data sets: (1) W, ρ and ρ' were estimated using entire EEG recording; (2) W – using first half, and ρ and ρ' – second half of EEG recording; (3) W – using second half, and ρ and ρ' – first half. These estimations of ρ and ρ' were performed for each EEG recording and averaged for each combination and for the EO and EC conditions separately.

Both ρ and ρ' quantities are probably biased estimates with respect to the random sample size. The lower limit values of these quantities for random sample size, corresponding to the real EEG recording, were assessed using simulated independent stochastic time series with autocorrelation function, similar to the EEG processes. These stochastic time series were simulated by 100-th order autoregressive (AR) models which parameters were estimated (Akaike, 1969) using arrays of the EEG recordings re-filtered to 1.5–40 Hz frequency band.

2.4. Spectral and statistical analysis

Spectral analysis was performed for the raw EEG, the CSD, the gIC^{EO} and the gIC^{EC} separately. For each individual, each condition and each component (EEG channel) power spectra were computed separately as follows. The continuous EEG data were segmented into 4.096 s epochs (50% overlap). All epochs containing artifact were removed from analysis. The spectral power density was computed using a Hanning window and fast Fourier Transform (FFT) and averaged across epochs. Power spectra with a number of averaged epochs less than 10 were eliminated from further analysis. Therefore, the numbers of subjects were slightly different for the EO and EC conditions. The absolute power were computed for δ (1.5–4 Hz), θ (4–8 Hz), α (8–13 Hz), $\beta 1$ (13–20 Hz) and $\beta 2$ (20–30 Hz) frequency bands, and transformed using logarithm for normalization before further statistical analysis. The grand average power spectra were computed for each component (EEG channel), each group of subjects and each condition separately.

A two-way ANOVA with between-subjects factor "Group" (ADHD vs. control) and within-subjects factor "Location" (Fp1, Fp2,...) was used to evaluate the differences between EEG power in ADHD patients and healthy subjects for each frequency band separately. Similarly, a two-way ANOVA with between-subjects factor "Condition" (EO vs. EC) and within-subjects factor "Location" was used to compare the spectral power for the EO and EC condition. For violations of sphericity, Greenhouse-Geisser corrections to the degrees of freedom were applied. These methods of analysis were used only for the power spectra of the raw EEG and the CSD, because their application to the power spectra of the gIC^{EO} and the gIC^{EC} may give ambiguous results due to arbitrary normalization of components.

To explore the location of differences of EEG spectral characteristics between ADHD patients and healthy controls or between the EO and EC conditions spectral power was compared by t-criteria for each type of data, each frequency band and each component (EEG channel) separately. Bonferroni correction was applied to eliminate false positive errors, i.e. results were reported with $p < 0.01/95 = 0.000105$. To quantify the effect sizes of differences of EEG spectral characteristics the Cohen's d was computed.

2.5. Equivalent sources localization

Following the studies of different authors (Onton and Makeig, 2006; Grin-Yatsenko et al., 2010; Congedo et al., 2010b; Makeig and Onton, 2012) the topographies from gICA models were fitted by equivalent dipole sources or by equivalent source current density in order to locate possible sources of the gIC. The four-shell spherical volume conductor model of the brain was used for localization of equivalent dipole source (Sun, 1997). The current density distribution corresponding to the topography of component was estimated using sLORETA inverse solution that models the brain by a three-shell spherical head model registered to the Talairach human brain atlas (Pascual-Marqui, 2002).

3. Results

The estimation of the optimal order of gICA model of EEG was performed using ITC (AIC, KIC and MDL) for the EO and EC condition separately using a regular and random decimation of the data with subsampling depth from 5 to 1000. All ITC were monotonically decreasing functions of the number of components for the EO condition regardless of the degree of decimation, and for the EC condition in the case when the subsampling depth was less than 100. However, ITC could have a local minimum for the EC condition in a relatively small number of cases, if degree of decimation was larger than 100. Thus, these results indicate only approximately that the optimal order of gICA model is probably equal to 19 for both EO and EC conditions. In the case of iICA, the results of application of ITC were strongly dependent on the subsampling depth and duration of the EEG recording. However, the optimal order for iICA model was equal to 19 in most cases (>95%) if the subsampling depth was smaller than 10.

Topographies for the gIC^{EO} (A) and the gIC^{EC} (B) models obtained for EEG in healthy subjects are shown in the upper part of Fig. 1. Despite the fact that these models are not identical (indices of topographies similarity $r_{ii}^{EO,EC}$ for 19 pairs of components are presented in Table 2), there are common features. For both models the topography of component (named as cFz) with largest variance have maximum at Fz. Its influence extends to all electrodes. Other 18 components have more local effects. However, the topographies of all components are spatially distributed so that their signals influence on several neighboring electrodes. Most of topographies have one local maximum which is located near the corresponding electrode. Sometimes the topographies could also have additional minor local minimum, but usually the estimation accuracy of such components are relatively low (see Table 2) in accordance with the *Reliability test 5*. In general, both gIC^{EO} and gIC^{EC} models are approximately symmetric with respect to the median line of brain, i.e. some topographies are symmetric, others form a symmetrical pair. The cFp2 component for the EC condition (Fig. 1B) is considered here as an exception because of its topography is antisymmetric.

At least two effects were observed when the dimension of the data was reduced to 4–18 components. First, the gICA models were often not symmetrical with respect to the median line. Second, many gICA models included components with antisymmetric topographies, and their spatial form varied from case to case.

Estimation accuracy of the iICA models is apparently very low in accordance with the *Reliability test 1*: $\bar{\tilde{r}} = 0.76$ ($\sigma_r = 0.05$) and $\overline{P_{0.95}} = 26.6\%$ ($\sigma_P = 17.9$) for the EO condition, and $\bar{\tilde{r}} = 0.77$ ($\sigma_r = 0.05$) and $\overline{P_{0.95}} = 32.5\%$ ($\sigma_P = 16.5$) for the EC condition. The spatial form of topographies of the iICA models varied greatly. Some of the topographies were broadly spatially distributed patterns, others were more local, and these differences were mostly random both within and between subjects. Nevertheless, the whole set of iICA models can be divided into three groups using visual analysis. The iICA models were assigned to the first group (19% for the EO and 24% for the EC condition), if only one well-defined local maximum was observed on each topography, and these extremes were located near the electrodes (similarly to that shown in Fig. 1A). The second group included those iICA models (69% for the EO and 63% for the EC condition), in which almost all the topographies of components had similar properties as described above, but 1–3 low power components had topographies with complex spatial structure, i.e. several local extremes were observed. The third group included those iICA models (12% for the EO and 13% for the EC condition), in which many (more than 3) topographies of components had a complex spatial structure.

The iICA and gICA models were quite similar: most of the topographies had local maxima near the electrodes. In some cases, corresponding topographies were wider in the iICA models, and in other cases – in the gICA model. However, most of the topographies from the gICA models (excepting the cFz component) were slightly less spatially distributed in comparison with corresponding topographies from the iICA models. In contrast, the topography of the cFz component from the gICA model was more spatially distributed. Also, the percent of power for the cFz component from the gICA models was at least two times greater than average percent of power of corresponding components from the iICA models.

The results of reliability analysis of the gICA models are presented in Table 3. The *Reliability test 2* indicates that highly reliable gICA models ($\bar{\tilde{r}} > 0.99$ and $\overline{P_{0.95}} > 99\%$) can be obtained if total

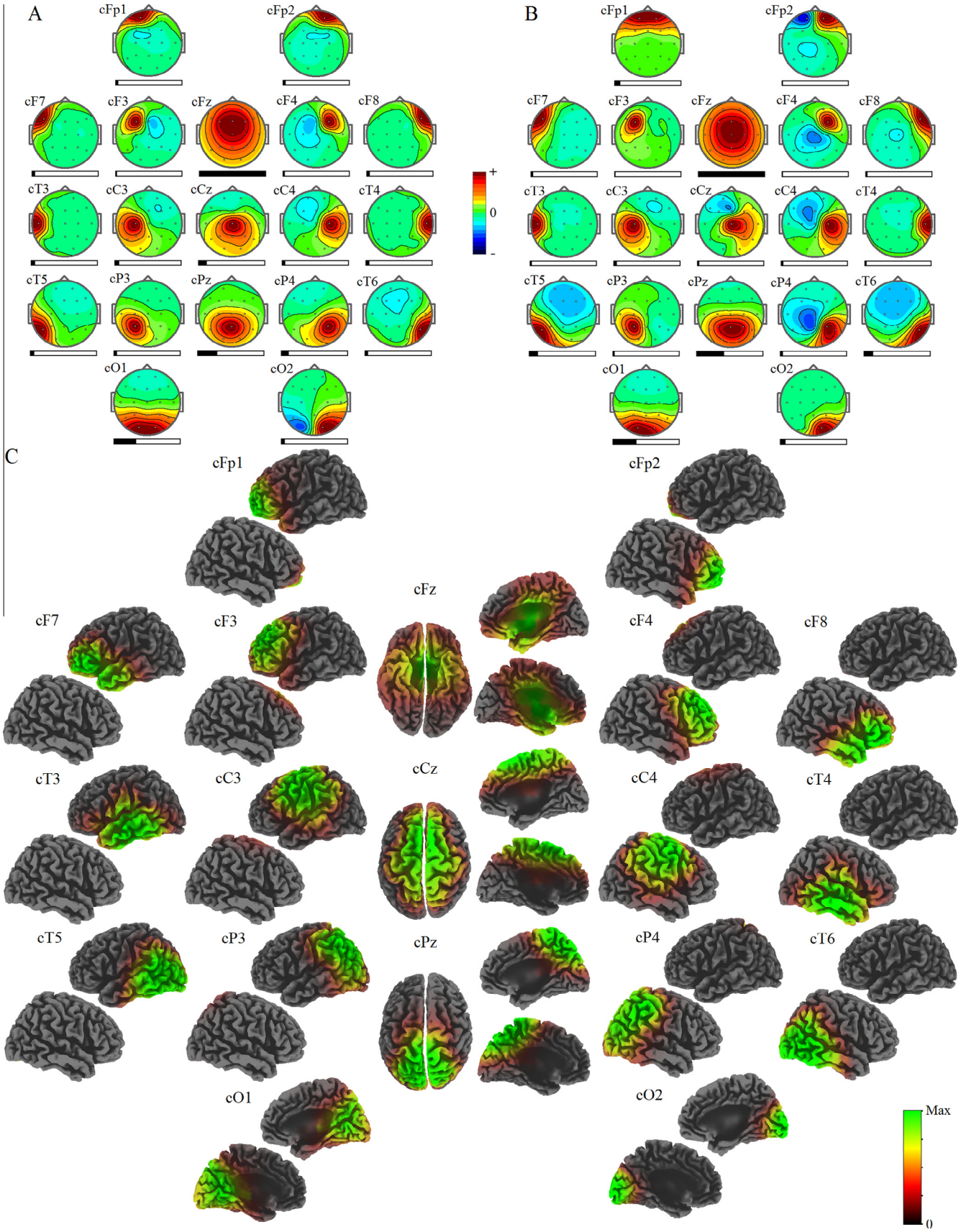

Fig. 1. Topographies of components for the gIC^{EO} (A) and the gIC^{EC} (B) models. Horizontal bars below the maps partially filled with black indicate the ratio of power of components relative to each other. (C) sLORETA current density distribution for each topography from the gIC^{EO} model.

Table 2
The comparison of the gIC^{EO} and the gIC^{EC} models, and the results of sLORETA source localization for the gIC^{EO} model.

	gIC^{EO} %P	$\overline{r_{ii}^{12}} \pm \sigma_{ii}$	gIC^{EC} %P	$\overline{r_{ii}^{12}} \pm \sigma_{ii}$	$r_{ii}^{EO,EC}$	BA	Gyrus
cFp1	1.8	0.989 ± 0.009	3.5	0.993 ± 0.008	**0.62**	10 (L)	Superior frontal gyrus
cFp2	1.7	0.979 ± 0.023	0.6	**0.933 ± 0.035**	**0.71**	11 (R)	Superior frontal gyrus
cF7	1.8	0.993 ± 0.008	1.5	0.978 ± 0.027	0.95	47 (L)	Inferior frontal gyrus
cF3	1.0	**0.894 ± 0.172**	0.5	0.971 ± 0.033	0.85	9 (L)	Superior frontal gyrus
cFz	39.0	0.999 ± 0.001	38.6	0.999 ± 0.001	0.99	25 (R)	Anterior cingulate
cF4	1.2	**0.871 ± 0.178**	0.6	**0.782 ± 0.187**	0.93	10 (R)	Superior frontal gyrus
cF8	1.8	0.986 ± 0.018	1.2	0.939 ± 0.069	0.95	47 (R)	Inferior frontal gyrus
cT3	2.5	0.998 ± 0.001	1.1	0.994 ± 0.005	0.98	21 (L)	Middle temporal gyrus
cC3	2.7	0.992 ± 0.006	1.8	0.986 ± 0.012	0.99	6 (L)	Precentral gyrus
cCz	4.9	0.990 ± 0.011	1.2	**0.834 ± 0.063**	**0.81**	6 (R)	Superior frontal gyrus
cC4	2.0	0.989 ± 0.009	1.5	0.972 ± 0.024	0.96	6 (R)	Middle frontal gyrus
cT4	2.2	0.998 ± 0.002	1.1	0.995 ± 0.006	0.97	21 (R)	Middle temporal gyrus
cT5	2.3	0.983 ± 0.018	5.1	0.989 ± 0.016	0.85	22 (L)	Superior temporal gyrus
cP3	2.0	0.984 ± 0.033	1.2	**0.884 ± 0.204**	0.92	40 (L)	Inferior parietal lobule
cPz	11.5	0.994 ± 0.011	16.2	0.988 ± 0.016	0.97	5 (R)	Paracentral lobule
cP4	4.4	0.971 ± 0.097	1.6	**0.752 ± 0.236**	**0.64**	40 (R)	Inferior parietal lobule
cT6	2.0	0.987 ± 0.013	5.5	0.988 ± 0.016	0.90	21 (R)	Middle temporal gyrus
cO1	13.1	0.989 ± 0.011	14.0	0.995 ± 0.007	0.98	23 (R)	Posterior cingulate
cO2	2.1	**0.775 ± 0.240**	3.2	**0.940 ± 0.137**	0.87	17 (R)	Cuneus

%*P* – the percent of total power for each independent component from the gIC^{EO} and the gIC^{EC} models. $\overline{r_{ii}^{12}} \pm \sigma_{ii}$ – average reliability index for the topography of component and its standard deviation according the *Reliability test 5*. The cases with low reliability of topographies of component ($\overline{r_{ii}^{12}} < 0.95$) are highlighted by bold. $r_{ii}^{EO,EC}$ – the indices of topographies similarity between components in the gIC^{EO} and the gIC^{EC} models. The most significant differences are highlighted by bold. BA and Gyrus – Brodmann areas and names of the brain gyrus in which the global maxima of the current density distribution (computed by sLORETA for the gIC^{EO} model) are located.

Table 3
gICA models reliability.

	gIC^{EO}			gIC^{EC}		
Reliability test 2: Random selection of time intervals with duration TI from individual EEG.						
TI per subject	$\bar{\bar{r}} \pm \sigma_r$	$\overline{P_{0.95}} \pm \sigma_p$	NS_e	$\bar{\bar{r}} \pm \sigma_r$	$\overline{P_{0.95}} \pm \sigma_p$	NS_e
2 s	0.950 ± 0.022	85.4 ± 8.0	415	0.926 ± 0.034	82.7 ± 10.9	440
5 s	0.960 ± 0.021	91.8 ± 6.2	1000	0.961 ± 0.024	92.6 ± 8.5	1100
10 s	0.980 ± 0.016	96.9 ± 3.6	1800	0.966 ± 0.023	94.8 ± 5.6	2100
20 s	**0.993 ± 0.0025**	**99.7 ± 0.7**	**3500**	0.975 ± 0.024	97.3 ± 3.5	4100
40 s	**0.995 ± 0.0024**	**99.8 ± 0.7**	**6400**	**0.994 ± 0.0033**	**99.4 ± 0.6**	**7800**
60 s	**0.995 ± 0.0014**	**100.0 ± 0**	**9300**	**0.994 ± 0.0032**	**99.5 ± 0.6**	**11,600**
Reliability test 3: Random selection of samples with probability p (Δt – averaged sampling interval).						
p, (Δt s)						
0.2, (0.02)	**0.999 ± 0.001**	**99.9 ± 0.2**	**3100**	**0.999 ± 0.0001**	**100.0 ± 0**	**4200**
0.04, (0.1)	**0.995 ± 0.005**	**99.3 ± 0.9**	**630**	**0.998 ± 0.0007**	**100.0 ± 0**	**840**
0.02, (0.2)	0.986 ± 0.010	98.1 ± 2.9	300	**0.996 ± 0.0014**	**99.9 ± 0.5**	**420**
0.01, (0.4)	0.971 ± 0.022	94.5 ± 6.9	150	**0.993 ± 0.0025**	**99.5 ± 1.6**	**210**
0.004, (1)	0.965 ± 0.022	88.5 ± 11.0	63	0.977 ± 0.021	96.4 ± 5.2	82
0.002, (2)	0.963 ± 0.022	87.2 ± 10.9	31	0.954 ± 0.022	88.6 ± 8.7	41
0.001, (4)	0.954 ± 0.027	82.3 ± 11.9	16	0.909 ± 0.036	77.5 ± 11.9	20
Reliability test 4: Random split-half of group of healthy subjects						
1.0, (0.004)	0.921 ± 0.024	87.9 ± 5.4	7600	0.901 ± 0.020	83.5 ± 6.9	10,400
Reliability test 4: Random split-half of group of ADHD patients						
1.0, (0.004)	0.929 ± 0.024	86.3 ± 6.0	3000	0.874 ± 0.036	72.4 ± 9.0	4500
Reliability test 4: Random split-half of combined group of healthy and ADHD subjects.						
1.0, (0.004)	0.949 ± 0.024	93.5 ± 3.5	10,600	0.919 ± 0.016	89.7 ± 4.9	14,900

$\bar{\bar{r}} \pm \sigma_r$ – average index of similarity of two mixing matrixes, and its standard deviation. $\overline{P_{0.95}} \pm \sigma_p$ – average percent of the total power of components, for which the $r_{ii}^{12} \geqslant 0.95$, and its standard deviation. NS_e – the number of samples per one element of mixing matrix. The cases with extremely high reliability of gICA models are highlighted by bold.

duration of combined time series is longer than 5000 s for the EO and 11,000 s for the EC condition. The *Reliability test 3* shows that the size of combined time series can be smaller if it includes approximately i.i.d. samples. Thus, highly reliable gICA models can be obtained, if combined time series contain at least 630 samples per one element of mixing matrix for the EO and 210 samples – for the EC condition. Perhaps these limits are overestimated because the effective length of EEG autocorrelation function is longer than corresponding averaged sampling interval Δt (see Table 3). Note that in all cases when the assessments of the gICA models were highly reliable the topographies of components were the same as that is shown in the Fig. 1 with a high degree of accuracy ($\bar{\bar{r}} > 0.99$).

The *Reliability test 4* showed relatively low values of indices $\bar{\bar{r}}$ and $\overline{P_{0.95}}$. These results do not allow us to draw an unambiguous conclusion that the obtained gICA models correspond to any group of subjects with a high degree of accuracy and should be considered as approximations.

The gICA models were also computed for the set of EEG recordings in ADHD patients and for the combined set of EEG recordings in both healthy subjects and ADHD patients. Corresponding values of the indices $\bar{\bar{r}}$ and $\overline{P_{0.95}}$ according to the *Reliability test 4* are

presented in Table 3. The topographies of the gICA models obtained for healthy subjects and for ADHD patients were similar within the accuracy of estimation: $\hat{r} = 0.93$ for the EO and $\hat{r} = 0.87$ for the EC condition. The topographies of the gICA models obtained for healthy subjects only and for combined group were practically identical: $\hat{r} = 0.993$ for the EO and $\hat{r} = 0.999$ for the EC condition.

To assess the compliance of the gICA models with different EEG recordings, we estimated mutual dependence of signals using the second order (ρ) and forth order (ρ') quantities. Results are displayed in the Fig. 2. Looking on the Fig. 2, several conclusions can be made. (1) The mutual dependence of the raw EEG signals was relatively large ($\rho \approx 0.5$ and $\rho' \approx 0.35$). (2) The transformation of the raw EEG into the gIC^{EO} or the gIC^{EC} reduced the dependence of signals for each individual EEG recording (Fig. 2C and D). On average, the dependence decreased by 5–6 times (Fig. 2A and B). (3) The transformation of the raw EEG into the CSD also reduced the dependence of signals. But it was slightly higher compared to the gIC^{EO} or the gIC^{EC}. (4) In the case of the gIC^{EO} or the gIC^{EC}, the dependence of signals was less than 0.1 on average, but greater compared to the simulated independent time series. It was approximately the same for the gIC^{EO} and the gIC^{EC} models, and did not differ between groups of subjects. (5) The quantity ρ for the gIC^{EO} or the gIC^{EC} was lower for the case of combined time series in comparison with individual EEG recording. Minimal value of ρ corresponded to the cases where the training and test combined time series was the same. (6) The quantity ρ' did not differ for both the individual EEG recording and the combined time series.

The structure of mutual dependence of the raw EEG was studied using ρ_{ij} and ρ'_{ij} coefficients (see Section 2). ρ_{ij} and ρ'_{ij} were calculated for each individual EEG recording separately and averaged over all subjects. This analysis showed that at least weak dependence of the EEG signals ($\rho_{ij} \approx 0.2$ and $\rho'_{ij} \approx 0.1$) exists between all pairs of channels. More strong dependence of EEG signals was observed only for a smaller subset of the channel pairs for which the electrodes are spatially located relatively close to each other. Very strong dependence ($\rho_{ij} > 0.8$ and $\rho'_{ij} > 0.7$) was observed only for some pairs of neighboring electrodes.

In the case of iICA, the mutual dependence of signals was estimated for different combinations of training and test data sets. When W, ρ and ρ' were estimated using entire EEG recording, the means and standard deviations of ρ and ρ' were smallest: $\rho = 0.003 \pm 0.001$, $\rho' = 0.025 \pm 0.012$ for both EO and EC conditions (the following notation is used here: $\rho = \overline{\rho} \pm \sigma_\rho$). When one half of EEG recording was used to estimate matrix W, and the other half to assess ρ and ρ', they were larger: $\rho = 0.036 \pm 0.013$, $\rho' = 0.037 \pm 0.024$ for the EO, and $\rho = 0.037 \pm 0.024$, $\rho' = 0.041 \pm 0.047$ for the EC condition. If matrix W^{EO} was used to transform the whole set of EEG recordings into the gIC^{EO}, they were even larger: $\rho = 0.076 \pm 0.024$, $\rho' = 0.050 \pm 0.024$ for the EO, and $\rho = 0.100 \pm 0.040$, $\rho' = 0.061 \pm 0.060$ for the EC condition. However, *these differences of two means* (*for* ρ or ρ') *are* usually *less* than two standard deviations. Similar results were obtained for the gIC^{EC}. So even if there are differences between gICA and iICA models, they are relatively small.

The current density distributions (sLORETA) corresponding to the topographies of the gIC^{EO} model are shown in Fig. 1C. Excluding the cFz component, the locations of maxima of the current density (see Table 2) approximately corresponded to the positions of electrodes on the scalp. The current density for the cFz component

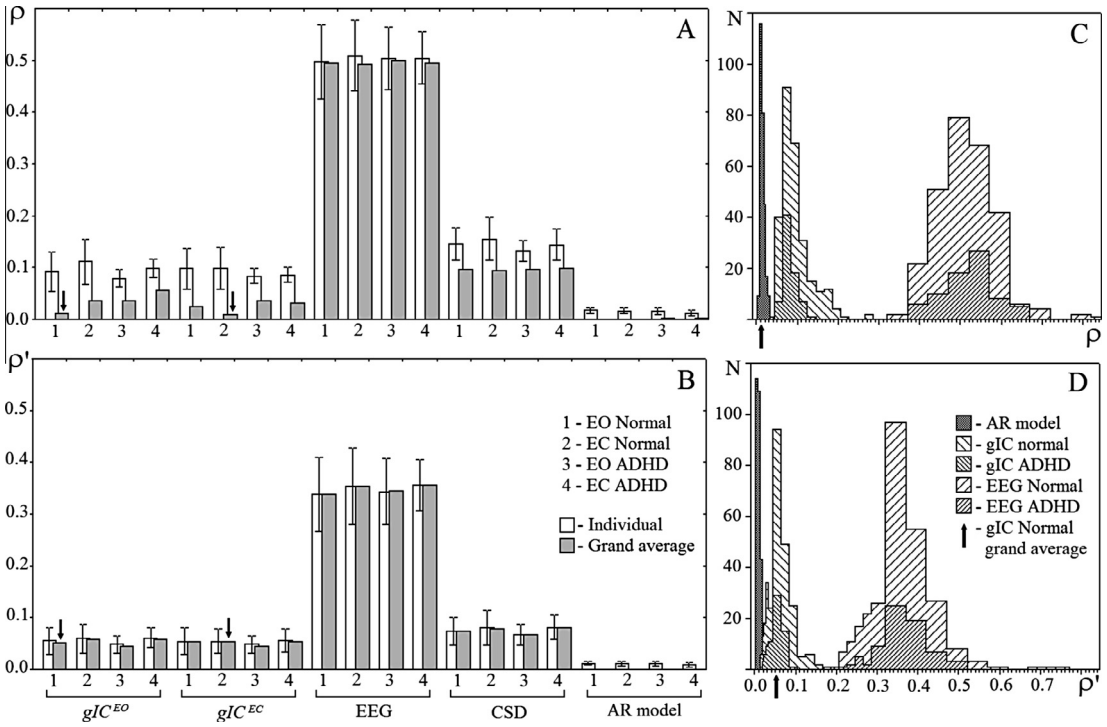

Fig. 2. Second (A) and fourth (B) order quantities (ρ and ρ') of mutual statistical dependency for different data. Digits along the horizontal axis correspond to different sets of the EEG recordings: 1 – healthy subjects, EO condition, 2 – healthy subjects, EC condition, 3 – ADHD patients, EO condition, 4 – ADHD patients, EC condition. Vertical bars marked as "gIC^{EO}" corresponds to gIC^{EO} model, "gIC^{EC}" – gIC^{EC} model, "EEG" – the raw EEG, "CSD" – the Current Source Density, and "AR model" – independent stochastic time series. Grey vertical bars correspond to the case, when ρ and ρ' were computed for combined time series, white vertical bars – for individual EEG recording separately and averaged; the whiskers represent one standard deviation above and below the mean. The down arrows indicate the cases when the training and testing combined time series were the same. The distribution histograms of ρ (C) and ρ' (D) for individual EEG recordings. "AR model" – the independent stochastic time series. "gIC normal" and "gIC ADHD" – the gIC^{EO} model of the EEG recorded in the EO condition in healthy subjects and in ADHD patients respectively. "EEG Normal" and "EEG ADHD" – the raw EEG recorded in the EO condition in healthy subjects and ADHD patients respectively. *X*-axis – the value of ρ (ρ'). *Y*-axis – the number of cases. The up arrows indicate the values of ρ and ρ' when the training and testing combined time series were the same.

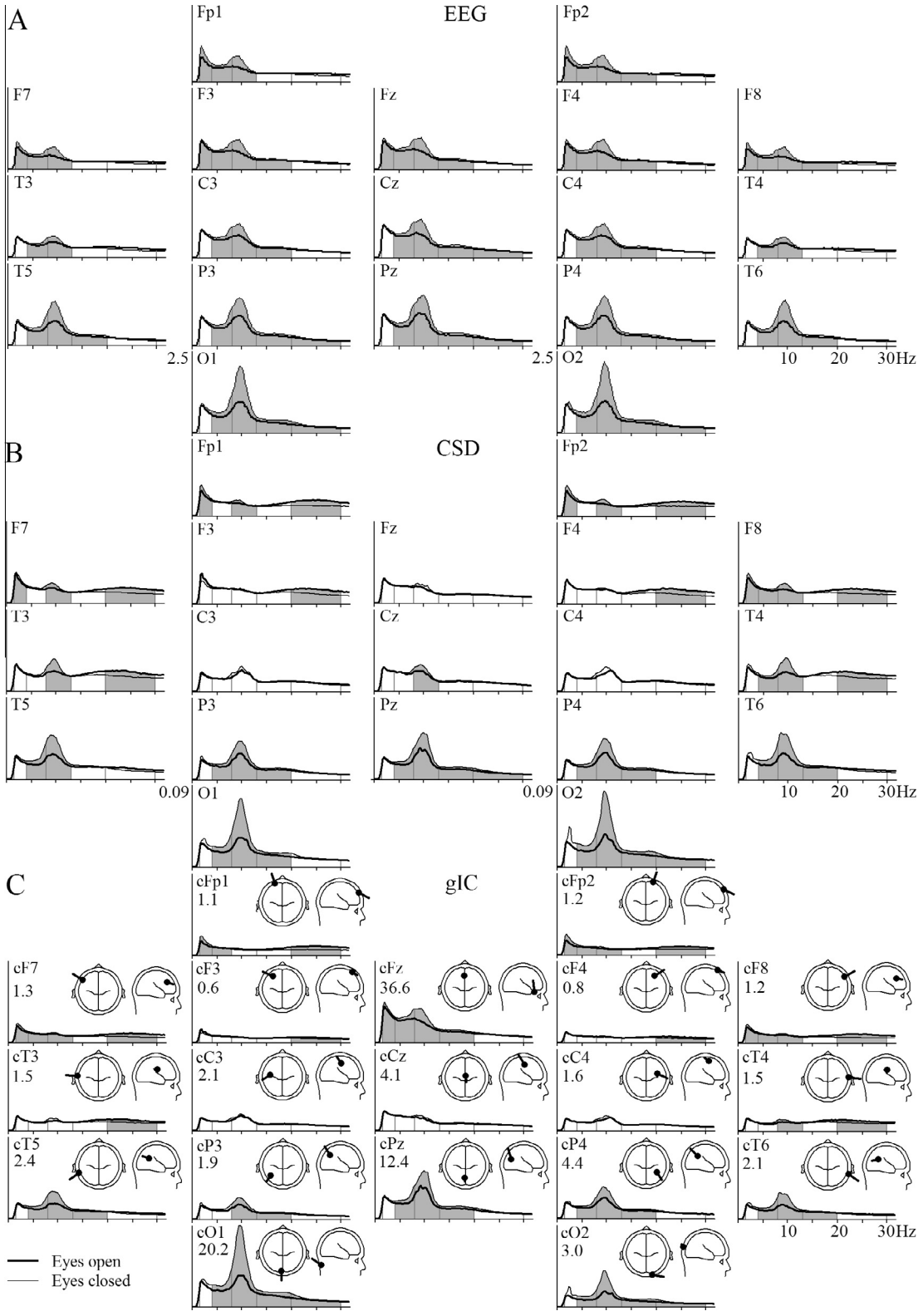

Fig. 3. Grand average power spectra of the raw EEG (A), the CSD (B), and the gIC^{EO} (C) in healthy subjects. Thick line – the EO condition, thin line – the EC condition. *X*-axis – frequency in Hz. *Y* axis – square root of power in μV (for A), or μV/cm^2 (for B), or conventional units (for C). The signals of the components (for C) are normalized in such a way that a maximal element of the topography for each component is equal to one. The gray color indicates the frequency ranges for which significant differences between the conditions ($p < 0.01$) were found. The name of electrode (component) is located in the upper-left corner of the graph, the percentage of total power, described by the component – below the name, the equivalent dipole source localization – in the upper-right corner of the graph.

was widely spatially distributed pattern located deep in the brain. Similar results were obtained for the EC condition. The topographies of components can be fitted by dipole sources with high accuracy according to the assessment of the relative residual energy (RRE < 0.1). The dipole locations usually correspond to the electrode positions. However, they are often outside the brain (see Fig. 3C).

The two-way ANOVA revealed significant differences between spectral power of the raw EEG and the CSD in the EO and EC conditions in both groups of subjects for each frequency band. Table 4 provides a list of significant results for the main effects and interaction. A more precise location of these differences was determined by comparing the spectral power for each electrode separately. It should be noted that the spatial-frequency pattern of the differences was similar in both healthy subjects and ADHD patients.

As seen in Fig. 3A, the increase in spectral power of the raw EEG for the EC condition in the δ range were observed only in the frontal areas, in the θ and α ranges – over the whole head, in the $\beta 1$ range – almost over the entire head, excepting some temporal sites and the left frontal electrode sites, and in the $\beta 2$ range – in the occipital, parietal and some central sites. In the case of the gIC^{EO}, most of the differences were also characterized by increased spectral power in the EC condition (Fig. 3C). However, the pattern of differences was more diverse. (1) The most considerable increase in spectral power seems to described by two groups of components: "anterior" group of components (cFz, cF7, cF8, cFp1 and cFp2) and "posterior" one (cO1, cO2, cP3, cPz, cP4, cT5 and cT6). (2) There were a number of components (cF3, cF4, cC3, cCz and cC4), for which the spectral power in δ, θ, α and $\beta 1$ ranges did not depend on whether the eyes were closed or open. (3) An increase of $\beta 2$ power was observed in the cP3, cO1 and cO2 components only. (4) Moreover, a decrease of spectral power in $\beta 2$ range was revealed in the cFp1, cFp2, cF7, cF8, cF3, cF4, cT3 and cT3 components. Similar picture was observed in the case of gIC^{EC} excepting the cFp1, cFp2 and cFz components. Here the increase of lower-frequency activity (δ and θ) was mainly observed in the cFp1 component, the increase of middle-frequency (α and $\beta 1$) – in the cFz and the decrease of higher-frequency ($\beta 1$ and $\beta 2$) activity – in the cFp2 component. These effects partially overlap in the frequency domain. The pattern of differences of the CSD spectra was largely similar to the case of the gIC^{EO} (see Fig. 3B and C), but not identical. (1) For the Fz electrode, the increase of power was not observed (Fig. 3B), while for the cFz components it was seen in a wide frequency range (Fig. 3C). (2) Both approaches revealed an increase of spectral power in θ and α ranges at anterior, central and temporal sites, but the spatial pattern was different.

There was found no statistically significant differences when comparing the spectral power using two-way ANOVA for the subtypes of ADHD patients, as well as for clinical and subclinical groups. For this reason, the power spectra of all patients were combined into one group. The two-way ANOVA revealed significant differences in spectral power of the raw EEG and the CSD between ADHD patients and healthy subjects, which are listed in Table 5. These differences were visually manifested as a reduction in spectral power in the group of ADHD patients and were identified for the raw EEG in δ, θ, α and $\beta 1$ ranges as the interaction of factors, and for the CSD in δ, θ, α and $\beta 1$ ranges – as main effects and interactions. However, no difference was found (at least for the chosen level of significance) between groups when comparing the spectral power of the raw EEG for each electrode separately.

Table 4
Two-ways ANOVA comparison of power spectra for the EO and EC conditions.

Frequency band	Healthy subjects			ADHD patients		
	Condition	Condition × Location		Condition	Condition × Location	
	F[1,581]	F[18,10458]	ε	F[1,158]	F[18,2844]	ε
Raw EEG						
δ	28.1**	60.1**	0.24	13.4**	19.2**	0.21
θ	47.1**	7.1**	0.22	18.5**	-	
α	161.4**	59.3**	0.17	46.0**	18.2**	0.21
$\beta 1$	43.1**	27.0**	0.31	-	8.0**	0.30
$\beta 2$	-	36.2**	0.32	-	12.8**	0.33
CSD						
δ	12.0**	10.3**	0.49	15.5**	3.9**	0.47
θ	25.5**	16.5**	0.34	12.6**	5.1**	0.31
α	88.6**	83.2**	0.32	32.5**	25.6**	0.27
$\beta 1$	–	31.1**	0.34	–	12.1**	0.30
$\beta 2$	12.5**	36.0**	0.32	8.0*	15.1**	0.32

* $p < 0.01$.
** $p < 0.001$.

Table 5
Two-ways ANOVA comparison of power spectra for groups of healthy subjects and ADHD patients.

Frequency band	EO			EC		
	Group	Group × Location		Group	Group × Location	
	F[1,349]	F[18,6282]	ε	F[1,390]	F[18,7020]	ε
Raw EEG						
δ	–	3.7*	0.29	–	3.5*	0.21
θ	–	4.0*	0.25	–	4.5*	0.20
α	–	4.9*	0.18	–	6.9**	0.17
$\beta 1$	–	–	–	–	3.5*	0.29
CSD						
δ	23.0**	–	–	18.34**	–	–
θ	19.4**	–	–	17.4**	–	–
α	9.4*	–	–	8.7*	–	–
$\beta 1$	–	–	–	10.6*	3.26*	0.34

* $p < 0.01$.
** $p < 0.001$.

The comparison of spectral power of the gIC^{EO} revealed a number of significant effects (see Fig. 4A and B). In all cases, these differences were manifested as the reduction of spectral power in the ADHD patients. Reduced power of signal for the cCz component in the frequency range from 1.5 to 20 Hz probably exists in both conditions. Although θ range is not highlighted in Fig. 4B, the statistical significance of this effect is rather high (t[390] = 3.88, $p < 0.012$ with Bonferroni correction). The reduction of spectral power for other components depended on whether the eyes were open or closed. Similarly, a significant reduction of the CSD spectral power in the ADHD patients was found at many electrode sites and in different frequency ranges, and varied depending on conditions (see middle row of diagrams in Fig. 4C, where significant differences correspond to Cohen's $d > 0.5$). However, the decrease in the spectral power for the Fz electrode in δ, α, $\beta 1$ and $\beta 2$ ranges was independent on conditions.

These results suggest that the transformation of the raw EEG into the gIC^{EO} or into the CSD significantly increases the sensitivity of the spectral analysis in detecting differences between healthy subjects and ADHD patients. This fact is illustrated in Fig. 4C, which shows the diagram of the effect size of differences (Cohen's d) between power of signals in healthy subjects and ADHD patients in five frequency ranges computed for the raw EEG, CSD and gIC^{EO}. It should be noted that the localization of changes in the spectral power is considerably different between the CSD and the gIC^{EO} cases. A similar increasing of the sensitivity of measurements was also observed in the case of transformation of the raw EEG into the gIC^{EC}. However, the localization of significant effects was a little different for frontal components in comparison with the gIC^{EO}.

It should also be noted also that statistically significant differences between the power spectra of the gIC^{EO}, the gIC^{EC} or the CSD have not been found for subgroups of patients with ADHD, as well as for clinical and subclinical groups.

4. Discussion

The results of these studies suggest that better sensitivity for discrimination of ADHD patients from normal subjects can be

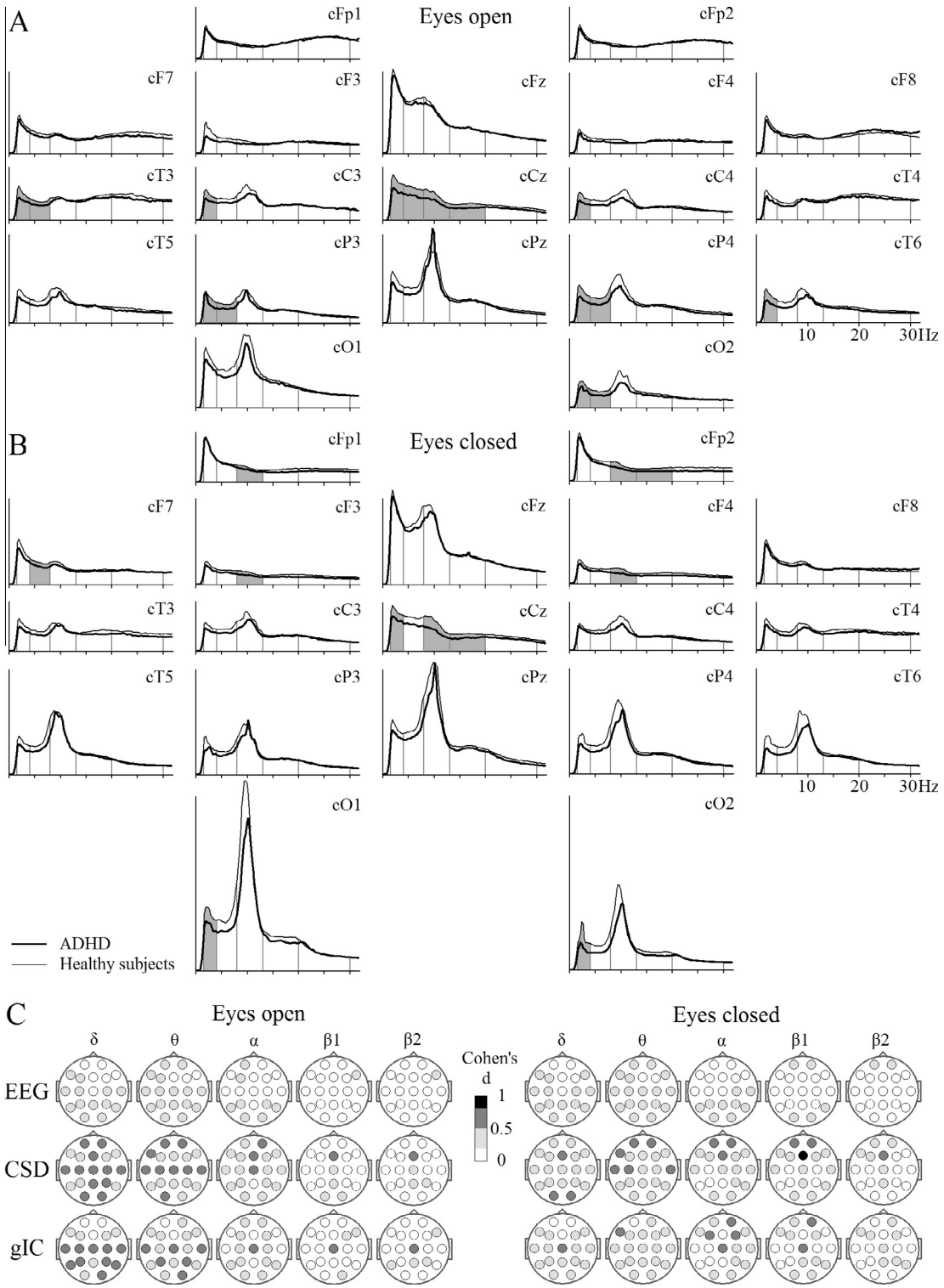

Fig. 4. Grand average power spectra of the gIC^{EO} in the EO (A) and the EC (B) conditions. Thick line – ADHD patients, thin line – healthy subjects. *Y* axis – square root of power in conventional units, the normalization of signals is the same as in Fig. 3. The gray color indicates the frequency ranges for which significant differences between the groups of subjects ($p < 0.01$) were found. (C) Diagrams of the effect size of differences (Cohen's *d*) in spectral power between healthy subjects and ADHD patients in five frequency ranges. Left set of diagrams correspond to the EO, right – the EC condition. Top row of the diagrams (EEG) corresponds to the raw EEG, middle row (CSD) – the CSD, bottom row (gIC) – the gIC^{EO}. On each of the diagrams, grayed circles topographically correspond to the location of graphs of the power spectra for the raw EEG, the CSD or the gIC^{EO}, as shown in Fig. 3 and 4. Value of the size effect is encoded using gray scale.

achieved using the spectral analysis of the gIC or the CSD in comparison the raw EEG. To interpret this formal statistical result, first consider the meaning of components in gICA model. In the conventional approach, some components are thought to be associated with brain signals, and others – with artifacts. However, this approach has limitations. For example, the typical waveforms corresponding to the mu rhythm are sometimes observed in the cC3 and cC4 components (see Fig. 1A). It would be logical to assume

that these components are associated with the mu rhythm. But such waveforms were not found in many other subjects, so it is difficult to be sure that these components are related primarily to mu rhythm. Several anterior components of gICA model cannot be associated with any well-known phenomena, because the properties of the reactivity of these brain areas are not well understood. The relationship of the component with the artifacts is not shown clearly. For example, the cFp1 component for the EC condition (see Fig. 1B) may be considered as eye blinking artifact in accordance with the form of its topography and power spectrum. However, quite a large signal can be observed in this component between eye blinks. This latter signal is not related to eye blinking, and hence, its exclusion from the analysis is unreasonable and will result in data loss.

Another point of view in the interpretation of components is also possible. Looking at the shape of topographies for the gIC^{EO} and the gIC^{EC} models and the sLORETA current density (Fig. 1), it is logical to assume that all the components, except the cFz, reflect some "local" portion of activity, which is generated near the electrode and which is weakly correlated with the signals from other areas. In contrast, the cFz component integrates some other highly correlated "global" portion of activity. Both "local" and "global" activity can represent not only the electrical potentials generated by neurons, but it may also include the other signals associated with artifacts such as EOG, EMG, etc. Therefore, it should be borne in mind that the group differences in spectral power may be related to artifacts which can be more powerful in one group of subjects as compared to another. Thus, the interpretation of the differences of spectral power for the raw EEG, the CSD, the gIC^{EO} or the gIC^{EC} seems to be very similar, except that most of the gIC related only to the "local" portion of activity. Also it should be noted that the inter-hemispheric asymmetries of spectral power of EEG activity cannot be assessed using gICA model because of the scale ambiguity.

The nature of highly correlated "global" portion of the activity is not clear. One possible factor is the referent that affects the signals from all electrodes. But, this assumption does not explain the form of topography of the cFz component. It could be also an internal cerebral process. Perhaps further study of its reactivity will shed light on the nature of this phenomenon.

Several indirect evidences indicate that the gICA model seem to be rather rough approximation, and that the main limitation is the number of components that cannot be greater than the number of electrodes.

(1) Typically, the ITC (AIC, KIC and MDL) are monotonically decreasing functions of the number of component. These results indicate that the actual number of independent factors can be greater than or equal to the number of sensors, since the minimum has not been found.
(2) Despite the fact that a very large amount of data is used to assess the mixing matrix A, the reliability of estimates is less than the maximum possible value in accordance with the *Reliability test 4*. Such a property can occur if the algorithm's objective function is ill-defined, or if it has multiple minima. This may occur either when the data are very noisy, or if the model does not accurately describe the data. The second explanation seems more probable (see below).
(3) Even when the training and test data sets are the same, the mutual dependence of the signals is still quite high (see Fig. 2). This is not a drawback of the algorithm, because the degree of signal separation was significantly better for the synthetic data (Anemüller et al., 2003). Moreover, the gIC^{EO} and the gIC^{EC} provide approximately equal degree of mutual dependence of signal if the training and test data sets are different (see Fig. 2). However, these two models differ considerably. These facts also indicate that the gICA models are an approximation.
(4) Just as it is described for the case of iICA (Onton and Makeig, 2006; Makeig and Onton, 2012; Delorme et al., 2012), the topographies of components for the gICA models have a relatively simple spatial structure, which can be fitted by the equivalent dipole source with high accuracy. And usually, most of the topographies have a single local maximum. But sometimes, these are components in which the topographies are antisymmetric with respect to the median line of the brain (the cFp2 component for the gIC^{EC}). The possible existence of a source with such properties is highly questionable. Since, similar topographies are often observed when the dimension reduction is performed using PCA, it is reasonable to think that the appearance of such components is a side effect of the InfoMax algorithm in the undetermined case.
(5) The gICA model includes one component (cFz), which describes a highly correlated "global" portion of the activity, and eighteen components associated with the "local" effects. But it would be logical to assume that such "local" activity should exist for each electrode. Then, if we take into account the existence of a "global" factor, the total number of components must be greater by at least one. Perhaps the "local" activity near the Fz electrode is integrated into the cFz component and is not available for analysis.
(6) Most of the topographies in the gICA models (excepting the cFz component) are slightly less spatially distributed in comparison with iICA models. The cFz component has the topography that is a considerably broader spatial pattern in the gICA models. Similar conclusions can be drawn by comparing the gICA models and the topography of components obtained by iICA for 71-channel EEG (Delorme et al., 2012). A detailed analysis of the mutual dependence between the EEG signals shows that at least weak correlation exists for all channel pairs. This fact suggests the presence of some additional "global" factor affecting all channels. Perhaps this factor is better fitted by the gICA models, and a very large amount of data is needed to separate it, because its effect is rather weak.

Our results indicate that the differences between the gICA and iICA models are relatively small, and the accuracy of the iICA model estimation is not enough for reliable detection the individual peculiarities of the spatial arrangement of the sources. These estimates confirm our assumption that the mixing processes is approximately the same in all subjects. However, this assumption may not be valid in the case of high-resolution EEG and it must be verified.

In fact, we have obtained two different gICA models: gIC^{EO} and gIC^{EC}. Both models seem to be equivalent in accordance with the assessment of how well they fit the different sets of data (see Fig. 2). Therefore, additional criteria are needed to determine which one is the best. One of these criteria may be an approximate symmetry of the gICA model relative to the median line of the brain. In other words, it is assumed that all topographies of components either should be symmetric or should form a symmetrical pair. The existence of unpaired asymmetric topographies, as well as antisymmetric topographies is considered unacceptable. Moreover, in accordance with the results of the *Reliability test 5* (see Table 2), it would seem preferable to choose the gICA model, wherein the topographies of the components have a single local maximum. The gIC^{EO} model meets these criteria to a greater extent. It is also likely that the gIC^{EC} is distorted to a greater extent in comparison with the gIC^{EO} because the EEG recordings for the EC condition

contain the small-amplitude signals associated with eye movements that are difficult to identify and exclude from the analysis.

Solution of the inverse problem is non-unique, so the results of source localization are typically very rough. In our case, many of the equivalent dipole sources are located outside the brain (Fig 3 B). This may be due to several reasons: (1) The source is distributed. (2) The localization error can occur as a result of edge effects, because of the source is located near the boundary of the electrodes grid. (3) The localization of the source can be biased by the influence of the referent. (4) The artifacts deform the topographies of the gICA model. According to our results (see Fig. 1), sLORETA is probably a more appropriate approach. Nevertheless, the results of sLORETA analysis may also be very imprecise due to the influence of these factors, and perhaps for these reasons, the current density distribution for the cFz component seems unlikely. But despite the low accuracy of these methods, they show that the sources of the components in the gICEO model (excluding the cFz) are located near the electrodes (see Fig. 1 and Fig 3C).

Looking at the shape of topographies in the gICA models, it can be concluded that one of the main factors that causes an interdependence of EEG signal, is the volume conduction. Then, one would assume that the transformation of the raw EEG into the CSD and into the gIC^{EO} or the gIC^{EC} would be equivalent. Indeed, there is a certain similarity in the power spectra for the CSD and the gIC^{EO} (see Fig. 3), and both these transformations allow to identify better the local effects in comparison with the analysis of the raw EEG. There are still also considerable differences. First, the transformation of the raw EEG in the CSD leads to a partial data loss (see Fig. 3B and Fig 3C), since the low-spatial-frequency components are attenuated (Hjorth, 1980). Second, the mutual dependence of signals for the CSD is slightly larger than for the gIC^{EO} or the gIC^{EC} (see Fig. 2). Finally, the patterns of differences in the spectral power between the two groups of subjects are dissimilar for cases of the gIC^{EO} and the CSD (see Fig. 4C).

In general, the results of comparison of the power spectra for the raw EEG, the CSD and the gIC^{EO} in the EO and EC conditions do not contradict each other. The increase in spectral power in α range in the posterior components for the EC conditions (Fig. 3C) seems to be related to the occipital alpha rhythm. Since this effect was observed in several components, one can assume that the occipital alpha rhythm is quite complex and heterogeneous phenomenon, that confirms the earlier findings (Tenke and Kayser, 2005). A considerable increase in α power is also observed in the cFz component. Perhaps this effect is related to the occipital alpha rhythm, but its location is not quite clear. One possible explanation is that some of the sources of the occipital alpha rhythm are close to the earlobes, and their signals affect the referent. It is also possible that the effects associated with the volume conduction were not completely suppressed because of the limited number of components. In order to clarify this issue, further studies with a large number of electrodes are needed. The increase in low-frequency power (δ, θ ranges) in the anterior components for the EC conditions is probably associated with the vertical and horizontal eye movements, because when the eyes are closed, the corresponding signals have small amplitude and they cannot be detected and eliminated as artifacts. A small increase in $\beta 2$ power in the frontal and temporal components, when the eyes are open, seems to be associated with a difference in the level of muscle activity in the EO and EC conditions.

Comparing the power spectra of the raw EEG between ADHD patients and healthy controls did not show any significant differences when the *t*-test was applied for each electrode separately. These findings confirm the results of the recently published study (Liechti et al., 2013), and support the conclusion that the spectral analysis of EEG at rest has a low sensitivity to discriminate ADHD from control groups. In contrast, significant reduction of spectral power in ADHD patients were identified in the different frequency ranges in cases of the CSD and the gIC^{EO} (Fig. 4), which are characterized by a "medium" effect size. The spatial pattern of differences depends considerably on the whether the eyes are open or closed, and the nature of this diversity is not fully understood. However, the spectral power in the range of 1.5–20 Hz for cCz component (identified in the case of the gIC^{EO}) and in the range of 1.5–4 and 8–30 Hz at Fz site (as revealed by CSD analysis) was considerably reduced in ADHD patients in both conditions. It is unlikely that these phenomena are related to the above described artifacts. According to sLORETA, sources for cCz component are located within Brodmann areas 5, 4, 6 and 8, near the median line of the brain (Fig. 1C), and the maximum of the current density is placed in Brodmann area 6. From the other hand, the radial component of current corresponding to the CSD at Fz site seems to be generated within Brodmann area 8. Because at least some of these regions are thought to be involved in the attentional processes (see for review di Michele et al., 2005), it is possible that the reduction of the activity of these brain areas might be a suitable marker for discrimination of ADHD adult and healthy subjects.

Acknowledgements

The authors wish to thank Stig Hollup, As. Prof., Department of Psychology of the Norwegian University of Science and Technology, Trondheim for providing us with EEG spectra obtained in healthy subjects.

References

Akaike H. Fitting autoregressive models for prediction. Ann Inst Stat Math 1969;21:243–7.
Akaike H. A new look at statistical model identification. IEEE Trans Auto Con 1974;19:716–23.
American Psychiatric Association. Diagnostic and statistical manual of mental disorders. 4th ed. Washington, DC.: American Psychiatric Association; 1994.
Anemüller J, Sejnowski TJ, Makeig S. Complex independent component analysis of frequency-domain electroencephalographic data. Neural Netw 2003;16:1311–23.
Barkley RA, Fischer M, Edelbrock CS, Smallish L. The adolescent outcome of hyperactive children diagnosed by research criteria: I. An 8-year prospective follow-up study. J Am Acad Child Adolesc Psychiatry 1990;29:546–57.
Barkley RA, Fischer M, Smallish L, Fletcher K. Young adult outcome of hyperactive children: adaptive functioning in major life activities. J Am Acad Child Adolesc Psychiatry 2006;45:192–202.
Barkley RA, Murphy KR, Fischer M. ADHD in adults. What the science says. Guilford Press; 2008.
Barry RJ, Clarke AR, Johnstone SJ. A review of electrophysiology in attention-deficit/hyperactivity disorder: I. Qualitative and quantitative electroencephalography. Clin Neurophysiol 2003;114:171–83.
Bell AJ, Sejnowski TJ. An information-maximization approach to blind separation and blind deconvolution. Neural Comput 1995;7:1129–59.
Biederman J, Petty CR, Monuteaux MC, Fried R, Byrne D, Mirto T, et al. Adult psychiatric outcomes of girls with attention deficit hyperactivity disorder: 11-year follow-up in a longitudinal case-control study. Am J Psychiatry 2010;167:409–17.
Bresnahan SM, Anderson JW, Barry RJ. Age-related changes in quantitative EEG in attention-deficit/hyperactivity disorder. Biol Psychiatry 1999;46:1690–7.
Bresnahan SM, Barry RJ. Specificity of quantitative EEG analysis in adults with attention deficit hyperactivity disorder. Psychiatry Res 2002;112:133–44.
Bresnahan SM, Barry RJ, Clarke AR, Johnstone SJ. Quantitative EEG analysis in dexamphetamine-responsive adults with attention-deficit/hyperactivity disorder. Psychiatry Res 2006;141:151–9.
Cao C, Slobounov S. Alteration of cortical functional connectivity as a result of traumatic brain injury revealed by graph theory, ICA, and sLORETA analyses of EEG signals. IEEE Trans Neural Sys Rehabil Eng 2010;18:11–9.
Cavanaugh JE. A large-sample model selection criterion based on Kullback's symmetric divergence. Stat Probab Lett 1999;44:333–44.
Chabot R, Serfontein G. Quantitative electroencephalographic profiles of children with attention deficit disorder. Biol Psychiatry 1996;40:951–63.
Clarke AR, Barry RJ, McCarthy R, Selikowitz M. EEG analysis in attention-deficit/hyperactivity disorder: a comparative study of two subtypes. Psychiatry Res 1998;81:19–29.
Clarke AR, Barry RJ, McCarthy R, Selikowitz M. EEG analysis of children with attention-deficit/hyperactivity disorder and comorbid reading disabilities. J Learn Disabil 2002;35:276–85.

Comon P. Independent component analysis, a new concept? Signal Process 1994;36:287–314.
Comon P, Jutten C, editors. Handbook of blind source separation: independent component analysis and applications. NY: Academic Press; 2010.
Congedo M, Gouy-Pailler C, Jutten C. On the blind source separation of human electroencephalogram by approximate joint diagonalization of second order statistics. Clin Neurophysiol 2008;119:2677–86.
Congedo M, John RE. D, Prichep L, Isenhart R. On the "dependence" of "independent" group EEG sources; an EEG study on two large databases. Brain Topogr 2010a;23:134–42.
Congedo M, John RE, Ridder DD, Prichep L. Group Independent Component Analysis of resting state EEG in large normative samples. Int J Psychophysiol 2010b;78: 89–99.
Debener S, Makeig S, Delorme A, Engel AK. What is novel in the novelty oddball paradigm? Functional significance of the novelty P3 event-related potential as revealed by independent component analysis. Brain Res Cogn Brain Res 2005;22:309–21.
Delorme A, Makeig S. EEGLAB: an open source toolbox for analysis of single-trial EEG dynamics. J Neurosci Methods 2004;134:9–21.
Delorme A, Palmer J, Onton J, Oostenveld R, Makeig S. Independent EEG sources are dipolar. PLoS One 2012;i7(2):e30135.
di Michele F, Prichep L, John ER, Chabot RJ. The neurophysiology of attention-deficit/ hyperactivity disorder. Int J Psychophysiol 2005;58:81–93.
Eichele T, Rachakonda S, Brakedal B, Eikeland R, Calhoun VD. EEGIFT: Group Independent Component Analysis for event-related EEG data. Comput Intell Neurosci 2011;2011:1–9.
El-Sayed E, Larsson JO, Persson HE, Rydelius PA. Altered cortical activity in children with attention-deficit/hyperactivity disorder during attentional load task. J Am Acad Child Adolesc Psychiatry 2002;41:811–9.
Faraone S, Biederman J, Mick E. The age-dependent decline of attention deficit hyperactivity disorder: a meta-analysis of follow-up studies. Psychol Med 2006;36:59–165.
Gittelman R, Mannuzza S, Shenker R, Bonagura N. Hyperactive boys almost grown up: I. Psychiatric status. Arch Gen Psychiatry 1985;42:937–47.
Grin-Yatsenko VA, Baas I, Ponomarev VA, Kropotov JD. Independent component approach to the analysis of EEG recordings at early stages of depressive disorders. Clin Neurophysiol 2010;121:281–9.
Groppe DM, Makeig S, Kutas M. Identifying reliable independent components via split-half comparisons. Neuroimage 2009;45:1199–211.
Hermens DF, Williams LM, Lazzaro I, Whitmont S, Melkonian D, Gordon E. Sex differences in adult ADHD: a double dissociation in brain activity and autonomic arousal. Biol Psychol 2004;66:221–33.
Hjorth B. An on-line transformation of EEG scalp potentials into orthogonal source derivations. Electroencephalogr Clin Neurophysiol 1975;39:526–30.
Hjorth B. Source derivation simplifies topographical EEG interpretation. Am J EEG Technol 1980;20:121–32.
Hung CI, Wang PS, Soong BW, Teng S, Hsieh JC, Wu YT. Blind source separation of concurrent disease-related patterns from EEG in Creutzfeldt-Jakob disease for assisting early diagnosis. Ann Biomed Eng 2007;35:2168–79.
Hyvärinen A, Oja E. Independent component analysis: algorithms and applications. Neural Netw 2000;13:411–30.
Hyvärinen A, Ramkumar P, Parkkonen L, Hari R. Independent component analysis of short-time Fourier transforms for spontaneous EEG/MEG analysis. Neuroimage 2010;49:257–71.
Iriarte J, Urrestarazu E, Artieda J, Valencia M, Levan P, Viteri C, et al. Independent component analysis in the study of focal seizures. J Clin Neurophysiol 2006;23:551–8.
James CJ, Hesse CW. Independent component analysis for biomedical signals. Physiol Meas 2005;26:R15–39.
Kayser J. Current Source Density (CSD) Interpolation using spherical splines: CSD toolbox (Version 1.1). New York State Psychiatric Institute: Division of Cognitive Neuroscience; 2009. Available at: http:// psychophysiology.cpmc.columbia.edu/Software/CSDtoolbox.
Kayser J, Tenke CE. Principal components analysis of Laplacian waveforms as a generic method for identifying ERP generator patterns: I. Evaluation with auditory oddball tasks. Clin Neurophysiol 2006a;117:348–68.
Kayser J, Tenke CE. Principal components analysis of Laplacian waveforms as a generic method for identifying ERP generator patterns: II. Adequacy of low-density estimates. Clin Neurophysiol 2006b;117:369–80.
Koehler S, Lauer P, Schreppel T, Jacob C, Heine M, Boreatti-Hümmer A, et al. Increased EEG power density in alpha and theta bands in adult ADHD patients. J Neural Transm 2009;116:97–104.
Kopřivová J, Congedo M, Horáček J, Praško J, Raszka M, Brunovský M, et al. EEG source analysis in obsessive–compulsive disorder. Abstracts, 16th Biennial IPEG Congress, 7–10 Oct 2010, Prague, Czech Republic.
Lazzaro I, Gordon E, Whitmon S, Plahn M, Li W, Clarke S, et al. Quantified EEG activity in adolescent attention deficit hyperactivity disorder. Clin Electroencephalogr 1998;29:37–42.
Leal A, Dias A, Vieira J. Analysis of the EEG dynamics of epileptic activity in gelastic seizures using decomposition in independent components. Clin Neurophysiol 2006;117:1595–601.
Li YO, Adalı T, Calhoun VD. Estimating the number of independent components for functional magnetic resonance imaging data. Human Brain Mapp 2007;28: 1251–66.
Liechti MD, Valko L, Muller UC, Dohnert M, Drechsler R, Steinhausen H-C, Brandeis D. Diagnostic value of resting electroencephalogram in attention-deficit/ hyperactivity disorder across the lifespan. Brain Topogr 2013;26:135–51.
Loo SK, Hale TS, Macion J, Hanada G, McGough JJ, McCracken JT, et al. Cortical activity patterns in ADHD during arousal, activation and sustained attention. Neuropsychologia 2009;47:2114–9.
Makeig S, Bell AJ, Jung TP, Sejnowski TJ. Independent component analysis of electroencephalographic data. Adv Neural Inf Process Syst 1996;8:145–51.
Makeig S, Jung TP, Bell AJ, Ghahremani D, Sejnowski TJ. Blind separation of auditory event-related brain responses into independent components. Proc Natl Acad Sci U S A 1997;94:10979–84.
Makeig S, Onton J. ERP features and EEG dynamics: an ICA perspective. In: Luck SJ, Kappenman ES, editors. The Oxford handbook of event-related potential components. New York: Oxford University Press; 2012. p. 51–88.
Marques JP, Rebola J, Figueiredo P, Pinto A, Sales F, Castelo-Branco M. ICA decomposition of EEG signal for fMRI processing in epilepsy. Hum Brain Mapp 2009;30:2986–96.
Melissant C, Ypma A, Frietman EE, Stam CJ. A method for detection of Alzheimer's disease using ICA-enhanced EEG measurements. Artif Intell Med 2005;33: 209–22.
Milne E, Scope A, Pascalis O, Buckley D, Makeig S. Independent component analysis reveals atypical electroencephalographic activity during visual perception in individuals with autism. Biol Psychiatry 2009;65:22–30.
Müller KR, Vigário R, Meinecke FC, Ziehe A. Blind source separation techniques for decomposing event-related brain signals. Int J Bifurcat Chaos 2004;14:773–91.
Onton J, Makeig S. Information-based modeling of event-related brain dynamics. Prog Brain Res 2006;159:99–120.
Onton J, Westerfield M, Townsend J, Makeig S. Imaging human EEG dynamics using independent component analysis. Neurosci Biobehav Rev 2006;30:808–22.
Pascual-Marqui RD. Standardized low-resolution brain electromagnetic tomography (sLORETA): technical details. Methods Find Exp Clin Pharmacol 2002;24(Suppl. D):5–12.
Perrin F, Pernier J, Bertrand O, Echallier JF. Spherical splines for scalp potential and current density mapping. Electroencephalogr Clin Neurophysiol 1989;72:184–7.
Perrin F, Pernier J, Bertrand O, Echallier JF. Corrigenda EEG 02274. Electroencephalogr Clin Neurophysiol 1990;76:565.
Rissanen J. Modeling by the shortest data description. Automatica 1978;14:465–71.
Sarela J, Vigario R. Overlearning in marginal distribution-based ICA: analysis and solutions. J Mach Learn Res 2003;4:1447–69.
Spencer TJ, Biederman J, Mick E. Attention-deficit/hyperactivity disorder: diagnosis, lifespan, comorbidities, and neurobiology. Ambul Pediatr 2007;7:73–81.
Sun M. An efficient algorithm for computing multishell spherical volume conductor models in EEG dipole source localization. IEEE Trans Biomed Eng 1997;44: 1243–52.
Tenke CE, Kayser J. Reference-free quantification of EEG spectra: Combining Current Source Density (CSD) and frequency principal components analysis (fPCA). Clin Neurophysiol 2005;116:2826–46.
Vigário RN, Sarela J, Jousmaki V, Hamalainen M, Oja E. Independent component approach to the analysis of EEG and MEG recordings. IEEE Trans Biomed Eng 2000;47:589–93.
Wax M, Kailath T. Detection of signals by information theoretic criteria. IEEE Trans Acoust Speech Signal Process 1985;33:387–92.
Yao D. High-resolution EEG mapping: a radial-basis function based approach to the scalp Laplacian estimate. Clin Neurophysiol 2002;113:956–67.
Yeredor A. Second-order methods base on colors. In: Comon P, Jutten C, editors. Handbook of blind source separation: independent component analysis and applications. NY: Academic Press; 2010. p. 226–79.